CRISPR/Cas9 editing of the wheat iron sensor *TaHRZ1* confirms its conserved role in iron homeostasis and allocation in grains

Deepshikha Tyagi[1,2], Hamida Banoo[1,2], Varsha Meena[1], Riya Joon[1], Kanupriya Agrwal[1,3], Anil Kumar[1], Santosh B. Satbhai[4], Terri Long[5] and Ajay K Pandey[1*]

Author affiliations

[1]National Agri-Food Biotechnology Institute (Department of Biotechnology), Sector 81, Knowledge City, S.A.S. Nagar, Mohali, Punjab, India.

[2]Regional Centre of Biotechnology, Faridabad, India

[3]Department of Biotechnology, Panjab University, Chandigarh, India

[4]Department of Biological Sciences, Indian Institute of Science Education and Research (IISER) Mohali, India

[5]Department of Plant and Microbial Biology, North Carolina State University, North Caroline, Raleigh, USA

[*]*Corresponding author*

Dr. Ajay K Pandey, Scientist-F

National Agri-Food Biotechnology Institute (Department of Biotechnology), Sector 81, Knowledge City, Mohali-140306, Punjab, India.

Telephone: +91-1724990124

Email: pandeyak@nabi.res.in; pandeyak1974@gmail.com

ORCID iD**:** https://orcid.org/0000-0003-1064-139X

Running head: HRZ proteins and Fe homeostasis in wheat

Abstract

Plants rely on specialised sensing systems, including transcriptional regulators, to maintain iron (Fe) homeostasis. Among these, Hemerythrin RING Zinc finger (HRZ) proteins have emerged as key regulators of Fe homeostasis. In this study, six wheat HRZ homoeologs TaHRZ1 and TaHRZ2 were identified from rice HRZ sequences and mapped to chromosomes 1 and 3. These encode proteins with conserved N-terminal Hemerythrin (HHE) domains and C-terminal CHY-RING and Zn-ribbon motifs. Phylogenetic analysis grouped these genes into distinct clades, while expression profiling revealed strong root-specific and Fe-responsive expression patterns, indicating roles in nutrient sensing. Functional conservation was demonstrated by complementation of the Arabidopsis *bts-1* mutant, where both wheat genes restored normal Fe regulation. Full-length TaHRZ1 and TaHRZ2 interacted with members of wheat bHLH IVc transcription factors, while truncated versions lacking the RING domain did not, emphasising their conserved role in protein interactions. CRISPR-Cas9 editing of the conserved HHE3 domain in all the TaHRZ1 homoeologs, coupled with GRF4-GIF1 chimeric protein, achieved ~9% regeneration efficiency in wheat cultivar C306. Grain ICP-MS analysis indicated enhanced iron loading in the edited lines, particularly in the scutellum, suggesting improved iron partitioning compared to the wild type. Additionally, qRT-PCR revealed upregulation of *FIT* and *IRO3*, and downregulation of *IDEF1* in edited lines, supporting a central role for *TaHRZ1* in Fe homeostasis signalling. These findings position *TaHRZ1* as a valuable target for biofortification strategies to enhance Fe content in wheat grains.

Keywords: iron, wheat, ubiquitin ligase, iron mobilization, protein-protein interaction

Introduction

Iron (Fe) is among the essential micronutrients in plants that participate as catalytic cofactors in several key processes. Our limited understanding of many of the mechanisms involved in plant Fe homeostasis is a major obstacle to devising approaches for Fe biofortification of staple foods. Plants have developed two strategies to acquire Fe from the rhizosphere (Kobayashi and Nishizawa, 2012). Non-graminaceous plants utilize a reduction-based strategy (Strategy I), while gramineous plants, which include the most important staple grain crops, utilize a chelation-based strategy (Strategy II). The Fe uptake Strategy in I mode involves the release of protons into the rhizosphere by H^+-ATPases, resulting in acidification and increased Fe solubility (Santi and Schmidt, 2009). Subsequently, ferric (Fe^{3+}) is reduced to ferrous (Fe^{2}) by ferric chelate reductases (FCR). Arabidopsis, FRO2 (a membrane-bound FCR) is one of the eight members of the FRO protein family that serves this function (Robinson *et al.*, 1999) Lastly, Fe^{2+} is translocated across the plasma membrane into the cells by an Fe-regulated transporter (IRT1), a member of the zinc-regulated transporter (ZRT), IRT-like protein (ZIP) divalent metal transporter family (Connolly *et al.*, 2002). In contrast, Strategy II involves biosynthesis and releasing mugineic acid family phytosiderophores (PS) into the rhizosphere. Fe is then solubilized through complex formation with PS, and Fe^{3+}-PS complexes are transported into the root via (Palmer and Guerinot, 2009) transporters belonging to the Yellow-Stripe (YS) family of proteins (Curie *et al.*, 2001; Palmer and Guerinot, 2009) .

Fe is successively taken up by epidermal cells through IRON-REGULATED TRANSPORTER1 (IRT1). This membrane-bound transporter protein facilitates the movement of Fe as well as other metal ions such as Zinc, Manganese, and Cadmium. (Colangelo and Guerinot, 2004; Eide *et al.*, 1996; Vert *et al.*, 2002). Once absorbed, Fe binds to chelating molecules like nicotianamine and citrate, which assist in its transport into and

throughout the plant's vascular system.(Durrett *et al.*, 2007; Curie *et al.*, 2009). At the transcriptional level, a major transcription factor Fer-like iron deficiency-induced transcription factor (FIT) in *Arabidopsis thaliana* regulates the expression of various Fe uptake genes (Bauer *et al.*, 2007). Additionally, other regulators, especially the basic helix-loop-helix (bHLH) transcription factors, including bHLH38, bHLH39, bHLH100, and bHLH101, interact with FIT to enhance its activity (Yuan *et al.*, 2008). Thus, FIT acts as a regulatory hub and forms complexes with other proteins to activate target genes involved in Fe homeostasis.

Ubiquitination, mediated by E3 Ubiquitin ligases, has been shown to be an important mechanism for controlling the turnover of Fe transporters and transcription factors (TFs) (Barberon *et al.*, 2011; Dubeaux *et al.*, 2018; Maria N. Hindt *et al.*, 2017; Kobayashi *et al.*, 2013; Spielmann and Vert, 2021), thereby regulating the stability. Specifically, Hemerythrin-rich Really Interesting New Gene (RING)- and Zinc-finger protein (HRZ) in rice and its *Arabidopsis thaliana* homolog BRUTUS (BTS) and BRUTUS-like (BTSL1 and BTSL2) play a significant role in maintaining Fe homeostasis in plants (Rodríguez-Celma *et al.*, 2019; Gao et al., 2020). HRZ proteins form a subfamily of hemerythrin E3 ubiquitin ligases that are conserved from green algae to higher plants and bear distant homology mammalian F-box and Leucine-rich Repeat Protein 5 (FBLX5) proteins, a post-translational regulator of Fe homeostasis (Salahudeen *et al.*, 2009; Vashisht *et al.*, 2009). HRZ/BTS proteins are characterized by its combination of hemerythrin (HHE) domain repeats, which can bind Fe, and RING and zinc-finger motifs, commonly associated with protein-protein interactions and C-terminal ubiquitin ligase activity (Selote *et al.*, 2015). Distant homology searches reveal the presence of two HRZ (HRZ1 and HRZ2) in rice and three genes *BTS* and *BTS*-like homolog viz. *BTSL1*, *BTSL2* in Arabidopsis.

Previously, it was demonstrated that OsHRZ1 can affect the stability of bHLH transcription factors members involved in Fe uptake through its E3 ubiquitin ligase activity (Kobayashi *et al.*, 2019). In general, HRZ1/BTS proteins possess three HHE domains at the protein level, while BTSL proteins have only two HHE domains (Maria N. Hindt *et al.*, 2017; Kobayashi *et al.*, 2013) . Previous work has demonstrated that the deletion of the HHE domain does not impact the polyubiquitination activity of HRZ proteins, indicating that the ubiquitination function is conserved even in the absence of this domain (Kobayashi et al., 2013) However, removing the C-terminal domains, which included the RING domain, eliminated the ubiquitination activity. It has been speculated that, while the HHE domain does not affect ubiquitination activity, it could contribute to the overall function of HRZ proteins by enabling them to respond to metal status or affecting their regulatory roles in Fe homeostasis (Kobayashi *et al.*, 2013). Earlier, it was shown that BTS lacking the HHE domain could complement the bts-1 sensitive phenotype, suggesting its contribution to the instability of the protein (Selote, *et al.*, 2015). Additionally, selective mutation of the HHE region revealed that the Ist and IInd domains contribute to the BTS stability. Similarly, IRT1 was also shown to undergo ubiquitin-conjugate-mediated degradation mediated by Iron Degradation factor RING E3 ligase (IDEF1) (Dubeaux *et al.*, 2018; Shin *et al.*, 2013) These studies underscore the critical role of E3 ubiquitin ligases in regulating iron homeostasis and highlight the need for further investigation in important crop species.

Hexaploid wheat is a major global crop and a key target for micronutrient biofortification. Previously, our group identified a comprehensive set of Fe-responsive genes in wheat and uncovered several potential regulatory candidates (Kaur *et al.*, 2019). Therefore, functional analysis of wheat genes shall enable bioengineering key regulators to drive targeted strategies for Fe biofortification. Growth Regulating Factor 4 (GRF4), aided by its cofactor GIF1, enhances wheat transformation efficiency by promoting cell proliferation and

regeneration competency in tissue culture (Debernardi *et al.*, 2020). In the current study, we identified and characterized wheat HRZ homologs, *TaHRZ*1 and *TaHRZ*2, which encode conserved domain structures and exhibit strong root-specific and Fe deficiency-induced expression. Functional complementation in Arabidopsis and interaction with bHLH IVc TFs confirmed their role conserved in Fe signalling. Next, the CRISPR-Cas9-mediated editing of *TaHRZ*1, aided by GRF4 and its GIF1, enhanced grain Fe content without yield penalties. These findings highlight *TaHRZ*1 as a promising target for wheat biofortification.

Results

Identification, sequence and expression analysis of wheat HRZ genes

To identify candidate *TaHRZ* in hexaploid wheat, we used Arabidopsis BTS and rice *HRZ* protein sequences to perform a BLAST search against the Wheat Ensembl database. Our analysis identified three homoeolog genes on chromosomes 1 and 3, designated as *TaHRZ*1 and *TaHRZ*2. The full-length cDNAs of *TaHRZ1 and TaHRZ2* were 3732 and 3645 bp, respectively and were expected to encode proteins of 1237 and 1214 aa (**Figure S1**). These proteins contain three N-terminal HHE domains, and the C-terminal with the presence of zf-CHY, RING-UB, and Zn-ribbon domains (**Figure 1A**). *TaHRZ1* shared 58% identity with BTS1, and 78%, 77% with *OSHRZ*1 and *OsHRZ*2. Whereas the *TaHRZ*2 shared 53%, identity with BTS1, and 73% ,79% with *OSHRZ*1 and *OsHRZ*2. A Neighbour-joining phylogenetic tree constructed from *TaHRZ1* and *TaHRZ2* and the *Arabidopsis*, *Oryza sativa* homologs grouped them into the 1st and 2nd clades (**Figure 1B**). Expression analysis of *TaHRZ1* and *TaHRZ2* at the homoeolog-specific level revealed differential but tissue-specific patterns. In spike, stem, and root tissues, all three homoeologs (A, B, and D) of both genes were expressed, with markedly higher transcript levels detected in roots compared to

spike and stem (**Figure 1C**). Enriched expression in the root suggests a conserved and potentially critical role of *TaHRZ*.

To gain insight into *TaHRZ1* and *TaHRZ1* function, we examined their expression in root and shoot tissues at different time points in response to iron deficiency (–Fe). At 4 days (D) of Fe deficiency, in roots, both *TaHRZ1* and *TaHRZ2* expression were markedly higher in –Fe, whereas Fe resupply (R) decreased their expression to the level of expression under +Fe. At this point, a similar response was also observed in shoots (**Figure 2A and B**). In shoots, higher fold expression of *TaHRZ1* and *TaHRZ2* was observed when compared to roots (**Figure 2B**). In addition to this, the expression of *TaHRZ*s in wheat grains and tissue type suggested that *TaHRZ*1 is highly expressed at 21 days after anthesis (DAA) (**Figure 2C**). Additionally, both the *TaHRZ* genes were highly expressed in the pericarp region of the grain tissue (**Figure 2D**).

Wheat HRZs complement bts-1 and interact with bHLH IVc member proteins

Next, we checked the ability of both the wheat HRZs to rescue the Arabidopsis BTS function. Arabidopsis overexpressing *TaHRZ1* and *TaHRZ2* in the Arabidopsis *bts-1* mutant were generated, and multiple lines were confirmed for 6XHis-tagged fused HRZ protein by Western (**Figure S2A**). At the phenotypic level, under +Fe, the complemented lines (Ox-HRZ1, and Ox-HRZ2), Col-0 and *bts-1*, exhibited similar phenotypic root length responses, however under the -Fe condition the complementing line displayed short root than *bts*-1 mutant (**Figure 3A**). Measurement of root length under +Fe and –Fe suggest that both the wheat HRZs were able to rescue the bts-1 insensitivity under both the conditions (**Figure S2B**). In terms of shoot chlorophyll content, the *bts-1* leaves contained lower total chlorophyll content compared to Col-0, Ox-HRZ1, and Ox-HRZ2 under +Fe and under –Fe, however, the Ox-HRZ1 and Ox-HRZ2 exhibit lower total chlorophyll and Fe content than the

bts-1 mutant (**Figure 3B**). Consistently, ICP-MS analysis showed that the complemented (Ox-HRZ1 and Ox-HRZ2) also accumulated less iron than the *bts-1* mutant under iron-deficient conditions (**Figure 3C**). *bts-1* also exhibited intense Perls staining of the roots compared to the Col-0 and the complemented lines (**Figure 3D**). Earlier, the enhanced accumulation of Fe in *bts-1* mutant has been attributed to high FCR (Ferric chelate reductase) activity (Maria N Hindt *et al.*, 2017). Under +Fe conditions, FCR activity was similar in Ox-HRZ1, Ox-HRZ2, *bts-1* mutant and Col-0. In contrast, under –Fe *bts-1* mutant exhibited significantly higher iron reductase activity FCR activity than Col-0 or the complementing lines (**Figure 3E**). At the molecular level, *TaHRZ* genes expressed in *bts-1* could restore the expression of Fe-responsive genes, such as *FRO2*, *IRT1*, *PYE*, *NAS* and *FIT*, to levels similar to Col-0 (**Figure S3**). These results emphasise the conserved role of *TaHRZ* as a possible negative regulator for Fe homeostasis.

BTS interacts with multiple bHLH IVc proteins to modulate their stability (Li et al., 2021; Long et al., 2010; Selote, *et al.*, 2015). Therefore, we examined whether wheat HRZ proteins exhibit a conserved ability to interact with bHLH IVc proteins that had previously been identified from wheat (Kumar *et al.*, 2022). Expression of full-length TaHRZ proteins in yeast was confirmed by Western blot analysis (**Figure 4A)**. We then assessed individual interactions between TaHRZ and multiple bHLH and FIT TFs. Both the TaHRZ1 and TaHRZ2 were able to interact with all the bHLH and GFIT homologs from wheat as indicated by the growth on the drop-out media -AHLT(x-Gal) (**Figure 4B**). This suggests that *TaHRZ*-encoded proteins possess similar, conserved functional domains that facilitate these protein-protein interactions. Further, we tested these interactions in the absence of the RING and other Zn-finger domains, by performing yeast two-hybrid with the deleted version of the *TaHRZ* (tHRZ1/2). The truncated RING and other Zn-finger C-terminal regions (t-HRZ1/2) show no interaction with bHLH and FIT TFs (**Figure 4C**). Our results support the prior

observation of the importance of the RING and other Zn-finger domains for protein interaction (Kobayashi, *et al.*, 2013) . Collectively, these results indicate that the conserved interaction between BTS and HRZ proteins is independent of the plant species' iron acquisition strategy

***GRF4-GIF1 chimeric protein assisted* genome editing of the HHE domain**

The HHE domains in the N-terminal region of BTS are essential for protein stability (Pullin et al., 2025; Selote, et al., 2015). Disruption of these domains in rice HRZ mutants lead to enhanced Fe in grains (Kobayashi, *et al.*, 2013; *Pullin et al.*, 2025). Therefore, we utilized genome editing to investigate the functional role of the HHE domain encoded by TaHRZ1. To enhance the regeneration efficiencies in Indian wheat, we employed the GRF4-GIF1 chimeric protein for CRISPR-Cas9 editing. For genome editing, we targeted the HHE3 domain of the TaHRZ1 protein by testing two different guide RNAs (gRNA1 and gRNA2) (**Figure S4A**). Two single gRNA (20 bp) were tested, to target the HHE3 domain; however, only one (gRNA2) targeted at exon7 showed effective in vitro cleavage activity (**Supplementary S4B)**. This gRNA2 was cloned into the JD633 binary vector system and was driven by the *TaU6* promoter (**Figure 5B**). To test the efficiency of the GRF4-GIF1 module, we tested the wheat calli regeneration percentage for cultivars (cv.) Fielder and Indian wheat C306. The resulting construct was introduced into wheat embryogenic callus tissue via *Agrobacterium*-mediated transformation (**Figure S5A-J and Figure 5C)**. Sixteen independent lines (T_0) were generated and screened for the presence of the transgene using primer-specific PCR amplification (**Table S1 and Figure S6A and B**). The GRF4-GIF1 chimeric protein resulted in enhanced regeneration percentage capacity of the transgenics of up to ~8.8 and 6.4 % for Fielder and C306, respectively (**Table S2**). We conclude that the

expression of GRF4-GIF1 module significantly improved regeneration in the Indian wheat cv. C306 and facilitated the efficient recovery of the putative edited events.

Next, Putative edited lines were identified using the T7 Endonuclease*1* assay, performed on amplicons generated from leaf genomic DNA with primers flanking approximately 150 bp on either side of the gRNA target site (**Figure S6C**). Several putative edited lines from cv. Fielder (D1, D3 and D7) and C306 (C1, C3); and were used for detailed characterization. Putative edited events from the T_1 plants exhibited normal morphology and development, with no obvious growth penalties associated with editing or transgene expression (**Figure 5D**), indicating successful recovery and establishment of transgenic lines. Western blot analysis of protein extracts from T_1 leaf tissue confirms the presence of Cas9 in the four transgenic lines of cv. Fielder (**Figure 5E**).

For initial characterization, multiple amplicons derived from the shoot genomic DNA (from independent transgenics) were generated and subjected to Sanger sequencing. Sanger chromatograms from CRISPR-edited wheat lines of Fielder (D1, D3, D7) and C306 (C3, C11) were analyzed to detect indel mutations at the target site. Sanger sequencing of the HHE3 amplicons for the T_1 plants revealed indel distribution from 1.0 to 16 % for 1 bp deletion. For the 2 bp deletion, the distribution ranged from 1 to 39 % in both cultivars. A predominance of 7 and 11 bp deletions and/or substitutions (+1 bp) was also observed in a few of these lines. Additionally, a larger deletion of 12, 19, 22, and 23 bp was also observed in a few of the edited lines, indicating a frame shift in *TaHRZ*1 and rendering it nonfunctional. Indel frequencies were quantified from sequencing data, and high R^2 values indicated accurate and efficient genome editing in the selected lines **(Figure 6A)**. Indel contribution in these lines occurred near the PAM cleavage site (**Figure 6B)**. Altogether, the Inference of CRISPR Edits (ICE) scores correlated well with Sanger sequencing data, thereby confirming successful genome editing. Next, to check the representation of the edits at the T_1

plant stage, we subjected individual clones to Sanger sequencing (**Figure S7**). These results confirm the successful editing of TaHRZ1 in two genetically distinct wheat cultivars. Furthermore, our data validate the effectiveness of GRF4-GIF1 in promoting higher regeneration in hexaploid Indian wheat cv.C306, thereby enhancing the efficiency of genome editing in wheat.

The defect in TaHRZ1 perturbs Fe distribution in wheat tissue

Previous studies have shown that HRZ proteins regulate grain Fe content in rice grains; however, little is known about their role in controlling Fe spatial distribution within the grain (Kobayashi et al., 2013). Grain phenotype of CRISPR-edited lines from two wheat cultivars, Fielder and C306, compared to their respective non-edited controls. The edited lines showed no visible differences in grain morphology compared to controls **(Figure 7A).** To investigate the functional role of *TaHRZ1*, we analysed grain Fe accumulation patterns in *TaHRZ1* mutant lines. Perls staining and inductively coupled plasma mass spectrometry (ICP-MS) revealed that Fe distribution was notably altered in the mutants (**Figure 7B and Figure S8A**). In wild-type plants, Fe was predominantly localised in the aleurone layer and the chalaza region of the grain. However, in *TaHRZ1* mutants, Fe accumulation was significantly increased in the scutellum region of the grain, as reflected by the staining intensity. This may suggest a partitioning of Fe during grain filling. Grain Fe content showed a 1.52-fold to 1.96-fold increase in edited lines of the two wheat cultivars (**Figure 7C)**. The level of grain phytic acid (PA) varied slightly ~1.2-1.4 % in these transgenic lines **(Figure S8B)**. Interestingly, the molar ratios of Fe:PA were found to be higher for the seeds generated from the transgenic lines when compared to the non-transgenic (**Figure 7D**). At the physiological level, while the number of grains per spike remained unchanged, *TaHRZ1* mutants displayed an incremental increase in 1000-grain weight,

suggesting improved grain filling (**Figure 7E & F)**. Despite the altered Fe distribution, no phenotypic differences in overall plant height or shoot architecture were observed between wild-type and *TaHRZ1* mutant lines (**Figure 7G**). These findings imply that *TaHRZ1* disruption improves grain Fe loading without compromising yield-related traits, offering the potential for biofortification strategies to enhance micronutrient content.

TaHRZ1 influences the expression of Fe homeostasis genes

To further understand the molecular changes associated with *TaHRZ1* disruption, we examined the phenotypic response and expression of key Fe homeostasis regulators in *TaHRZ*-edited (ed-tahrz1) wheat lines. At the phenotypic level, the *ed-hrz1* lines (2 lines for each cv.) show less root growth under +Fe conditions, suggesting that TaHRZ1 could impact root growth (**Figure S9A**). SPAD analysis shows no major difference in the edited and non-edited seedlings under +Fe and –Fe conditions (**Figure S9B**). This could be due to enhanced expression of *TaHRZ2* in –Fe. The levels of *TaHRZ1* were markedly reduced in the edited lines and remained relatively stable under both +Fe and –Fe conditions (**Figure 8A**). Under +Fe conditions, the expression of *TaHRZ2* was not impacted in WT and edited lines of *TaHRZ1* (**Figure 8B)**.

In contrast, –Fe induces the expression of *TaHRZ2* in the edited lines, but this response was lower when compared to expression in WT seedlings **(Figure 8B)**. On similar lines, expression of the Fe Deficiency-Responsive Element Binding Factor 1 (*IDEF1)*, a transcription factor that typically functions upstream in Fe signalling also show reduced expression in the edited lines (**Figure 8C**). The suppressed expression of *TaHRZ2* and *IDEF1* during –Fe may reflect feedback regulation in response to altered Fe sensing or translocation dynamics caused by the loss of *TaHRZ1* function. Additionally, qRT-PCR analysis revealed a marked upregulation of *FIT* (FER-like Fe Deficiency-Induced

Transcription Factor) and IRO3 (Fe-related bHLH transcription factor 3) in roots and shoots of the edited lines compared to WT plants under Fe deficiency (**Figure 8D and E**). Interestingly, FIT showed high expression in edited lines even under +Fe conditions. Together, these data suggest that *TaHRZ1* plays a central role in maintaining Fe homeostasis by modulating the expression of both Fe uptake and regulatory genes.

Discussion

Fe is an essential micronutrient required for numerous physiological processes. However, its availability in the soil is often limited, and maintaining optimal Fe levels within plant tissues requires tight regulation. In graminaceous crops like wheat, Fe homeostasis is critical for plant development and ensuring sufficient micronutrient content in the edible grain parts to meet human nutritional needs. Our investigation into the role of *TaHRZ1*, a wheat homolog of the Fe sensor gene *HRZ*/*BTS*, sheds light on its central role in regulating Fe distribution and related gene networks in hexaploid wheat. Progress in wheat transformation has lagged behind that of rice and maize, primarily due to the complexity of its genome (Garbus *et al.*, 2015; Wulff and Dhugga, 2018) .One of the main challenges in wheat gene editing is low regeneration efficiency in current elite cultivars. To overcome this, researchers have employed morphogenetic proteins to enhance embryogenesis and improve regeneration efficiency across several crop species. In particular, the Baby-Boom (BBM) and WUSHEL (WUS2), WOUND INDUCED DEDIFFERENTIATION1(WIND1) proteins and their combination have significantly boosted transformation frequencies in crops (Iwase *et al.*, 2017; Laux *et al.*, 1996; Lowe *et al.*, 2018). GROWTH REGULATING FACTOR 4 (GRF4) and its cofactor GRF-INTERACTING FACTOR1 (GIF1) have been shown significantly improve efficiency and speed of regeneration in wheat, triticale, and rice, while also expanding the range of wheat genotype amenable to transformation (Debernardi *et al.*, 2020).

Therefore, we tested the GRF4-GIF1 module on wheat cv. C306. In our study, introducing the wheat GRF4-GIF1 module significantly enhanced the regeneration efficiency of calli, resulting in transformation efficiencies ranging from 6.4 % to 8.8% derived from two wheat cultivars i.e. cv. C306 and Fielder respectively. As reported earlier, one typically expects a boost in transformation efficiencies of more than 20% when combined with Cas9/gRNA delivery. GRF4-GIF1 transgenic plants were shown to be fertile, and no obvious developmental defects were observed. In our study, although the transformation efficiency was low, no negative impact was observed for the Indian cv. C306. Further, optimization of the wheat regeneration may be required to adapt and improve the regeneration efficiencies of the transformations. Nonetheless, adapting the GRF4-GIF1 chimeric protein for Indian wheat cv. C306 significantly enhances transformation efficiency compared to previous studies (Aggarwal *et al.*, 2018; Bhati *et al.*, 2016). This reinforces the utility of morphogenetic regulators, such as GRF4-GIF1, for enhancing regeneration efficiency in hexaploid wheat, irrespective of cultivar.

In Arabidopsis and rice, *BTS*, *BTSL1*, *BTSL2* and *HRZ* have been characterised as E3 ubiquitin ligases involved in the sensing and degradation of Fe-related transcription factors to maintain homeostasis. The wheat *TaHRZ1* fulfils a similar function, albeit with unique regulatory consequences. However, in wheat, the presence of three homoeologs introduces additional layers of complexity, and the high expression of all three in roots points to a root-specific role in Fe sensing and uptake regulation. Interestingly, while *atbts* mutants display growth defects under high Fe (Maria N. Hindt *et al.*, 2017), the wheat *TaHRZ1* mutants have not been explored for this condition yet; future studies may be required in this direction. One of the most interesting aspects of *TaHRZ1* disruption was the coordinated change in the expression of key Fe-regulatory transcription factors. Notably, *FIT* and *IRO3* were significantly upregulated in the edited lines. *FIT* is a central transcription factor in the Fe

acquisition pathway, particularly in dicots, but it also plays a conserved role in monocots(Filiz and Kurt, 2019; Maria N. Hindt et al., 2017; Selote et al., 2015). The rationale for increased expression of Fe homeostasis genes upon HRZ/BTS is conserved in monocots and dicots, including wheat. HRZ proteins act as repressors, so their absence derepresses downstream targets, and this mechanism may result in high expression of known targets such as IRO3 and FIT. Based on the evidence, it appears that HRZ functions are conserved across dicots and monocots (Li *et al.*, 2023).

Targeted editing of *TaHRZ1* led to striking changes in Fe distribution, with intense Perls staining observed in the scutellum region of the grain. This is particularly notable, as this tissue plays an essential role in nutrient mobilization during germination. The intense Perls stain in the scutellum suggests a disruption in long-distance Fe transport, likely due to altered regulatory control over the expression or activity of transporters. Interestingly, this accumulation did not lead to visible growth defects, indicating that *TaHRZ1* is dispensable for vegetative development under normal conditions but is vital for fine-tuning internal Fe movement, especially during seed development. The potential trade-off between enhanced nutrient content and plant fitness or yield is a key concern in biofortification approaches (Ofori *et al.*, 2022). In our study, *TaHRZ1*-edited lines maintained normal plant height and grain weight, suggesting that the growth processes remained unaffected. These findings highlight *TaHRZ1* as a promising target for improving grain quality without yield penalties, which is a major advantage in crop improvement programs. Out findings also raise the possibility that editing combinations of *TaHRZ1* and *TaHRZ2* may reveal further insights into redundant or complementary roles in Fe regulation. The ability to manipulate Fe distribution within the wheat grain without negatively impacting growth or yield is a significant step forward in biofortification. Current biofortification strategies often rely on overexpression of Fe transporters or chelators, which may result in imbalanced nutrient profiles or impaired

growth. (Pal *et al.*, 2021; Sperotto *et al.*, 2012). Our findings suggest that modulating internal Fe regulators like *TaHRZ1* can enhance Fe accumulation in nutritionally relevant grain tissues (e.g., scutellum) without such drawbacks.

Future efforts to gain insight into TaHRZ function include determining whether the increased Fe in the scutellum can be mobilised and utilized efficiently during germination . These efforts, together with further editing strategies (e.g., targeting vacuole Fe transporters or chelators) could potentially redirect Fe to the endosperm to improve its bioavailability further and improve germination under conditions of low Fe availability. Exploring the combined effects of *TaHRZ1* and *TaHRZ2* double editing could provide deeper insights into redundancy and specificity in the wheat Fe regulatory network. Multiplex gene editing for traits in hexaploid has been routinely used (Zaman *et al.*, 2019). Transcriptomic or proteomic analyses of edited lines could also reveal downstream targets of *TaHRZ1*-mediated regulation, specifically in grains.

Utilizing GRF4-GIF1 to increase transformation efficiency we have shown that *TaHRZ1* is a key regulator of Fe accumulation and Fe distribution in wheat. Moreover, we have shown that disrupting TaHRZ1 enhances Fe accumulation in grain scutellum without compromising yield-related traits. The accompanying changes in *FIT*, *IRO3*, and *IDEF1* expression highlight the central role of *TaHRZ1* in the Fe regulatory network. Altogether, this study provides insights into the molecular mechanisms underlying HRZ-mediated nutrient regulation and establishes genome editing of HRZ as a viable strategy for biofortifying wheat grains. These findings pave the way for developing nutrient-dense wheat varieties, addressing global micronutrient deficiencies and enhancing food security. These results provide a promising foundation for developing nutritionally enriched wheat varieties through precise genome editing strategies targeting endogenous regulators of micronutrient homeostasis.

Material and methods

Plant growth conditions

Hexaploid wheat cv. C-306 and Fielder were used for this study. Following an overnight stratification process at 4 °C in the dark, wheat seeds were allowed to germinate on Petri dishes lined with Whatman filter paper. Endosperms were extracted from 4 days old seedlings and cultivated in PhytaBoxTM containers using Hoagland's nutritional solution. Iron-deficient plants (-Fe) were treated with 1 µM Fe^{3+}- EDTA, whereas control plants (+Fe) were treated with 80 µM Fe^{3+}-EDTA without any changes to the amounts of other nutrients. The plants were grown in a controlled growth environment with a photon flux density of 300 µmol m^{-2} s^{-1}, at 21±1°C, 50–65% relative humidity, and a 16–8hour light-dark photoperiod. After eight days on +Fe or –Fe media, roots and shoots were taken from three biological replicates and promptly frozen in liquid nitrogen for further examination.

Phylogenetic study and in-silico identification of wheat HRZ genes

Protein sequences from *O. sativa* HRZ, *Arabidopsis* HRZ, and wheat HRZ were utilized for phylogenetic analysis. Arabidopsis protein sequence was used to retrieve these HRZ protein sequences from the entire wheat genome using BLAST search in the Plant ensemble through. The MUSCLE algorithm (Edgar, 2004) was used to align the putative IDs and protein sequences, and MEGAX software was used to create a rooted tree using the maximum likelihood method (Kumar *et al.*, 2018). The phylogenetic tree was created to show the HRZs of *O. sativa* and *Arabidopsis*, which are most related to wheat HRZ. The degree of sequence similarity between *TaHRZ* proteins led to their classification into four clades. *TaHRZ* proteins resemble *O. sativa* the most, followed by *Arabidopsis*. The conserved motif architecture of the *TaHRZ* transcripts was subsequently ascertained by analysing their gene structure. MEME was used to anticipate these conserved

motifs(Bailey *et al.*, 2015). *TaHRZ* and Arabidopsis both shared conserved N-terminal Hemerythrin (HHE) domains and C-terminal CHY-RING and Zn-ribbon motifs. Additionally, the Gene Structure Display Server (GSDS) was used to analyse the organization of the introns and exons of wheat HRZ and their homeologs (Hu *et al.*, 2015).

Arabidopsis complementation and experimental conditions

Using site-directed cloning, the *TaHRZ*1 (ORF : 3714 bp; TraesCS3A02G262700, 3645 bp) and *TaHRZ*2 (ORF: 3645 bp; TraesCS1A02G374800), which were strongly expressed, were cloned into the plant expression vector pCAMBIA1302 (pCAMBIA1302:*TaHRZ*1/*TaHRZ*2-His) at the *Bgl*II and *Spe*1 restriction sites. These constructs were introduced into Arabidopsis seedlings, or T-DNA insertion lines of atbts1 (SALK_016526) mutant, using *Agrobacterium tumefaciens* (GV3101) mediated transformation by the floral dip method (Zhang *et al.*, 2006). Multiple (7-10) independent transformants were screened on 0.5x MS media containing 30 mg/L hygromycin and 0.8 % agar. The transformed seedlings(T1) with long hypocotyls and green expanded leaves at a 4-leaf stage were separated from the non-transformed seedlings and transferred to the soil after about 3 weeks. Similarly, T_2 and T_3 generation seeds were also selected and allowed to grow till maturity. The transgenic seedlings were confirmed for the presence of recombinant cassette using PCR-based approach. The transgenic lines containing the empty pCAMBIA1302 vector were used as a control (WT). The PCR-positive lines, which showed Western blot positivity, were further used for functional characterisation.

Perls Staining and ICP-MS analysis

Hoagland's nutrient solution was used to grow wheat plants (*Triticum aestivum* L.) and Arabidopsis seedlings in a controlled setting. After five days of supplementation with B5 agar media, the plants were moved to B5 minimum media that had been altered with + Fe (control) and − Fe (deficiency) for an additional five days. Root samples taken after the

necessary developmental stage were used for Perl's Prussian Blue staining to evaluate Fe^{3+} accumulation. Root samples were vacuum-infiltrated for an hour in a dark environment to improve reagent penetration after being submerged in a solution containing 5% potassium ferrocyanide and 5% HCl. Following staining, the roots were carefully cleaned with deionized water to remove any remaining stains examined under a stereomicroscope. The development of a blue precipitate indicated the presence of Fe^{3+}.

Isolation of total RNA, cDNA synthesis, and quantitative real-time PCR analysis

RNA was manually isolated from diverse tissues using TRIzol® Reagent (Invitrogen™). To remove genomic DNA contamination, RNA samples were treated with TURBO™ DNase (Ambion, Life Technologies) after quantifying their integrity and concentration. Two micrograms of total RNA were used to synthesize cDNA as per the manufacturer's instructions using the Invitrogen SuperScript III First-Strand Synthesis System SuperMix (Thermo Fisher Scientific). QuantiTect SYBR Green RT-PCR Kit (Qiagen, Germany) was used for qRT-PCR. Oligocalc software was used to carefully designed separate set of gene-specific primers for TaHRZ1/TaHRZ2 genes to amplify a 150-250-bp area from all three homologous of each gene. *TaHRZ*1/*TaHRZ*2 genes. The experiment was validated using four technical replicates for each pair of primers and at least two to three experimental replicates. The ADP-ribosylation factor gene (*TaARF*) was an internal control in all the expression tests. The C_t values obtained after the run were normalised against the internal control, and relative expression was assessed using the $2^{-\Delta\Delta CT}$ method (Livak and Schmittgen, 2001). All the primers used in the study are mentioned in **Table S1**.

Design of guide RNA, Wheat transformation, screening and of TaHRZ1 edits and genotyping

The conserved region of all three homoeologs of *TaHRZ*1 was used for gRNA design. The gRNA spacers were designed using wheat CRISPR webtool (Breaking Cas software

https://bioinfogp.cnb.csic.es/tools/breakingcas/). We designed the gRNA to target a unique site in the 7th/8th exon of the *TaHRZ*1 gene that was a consensus site for all three homoeologs (**Table S1**). The *TaHRZ1* targeting gRNA construct prepared in JD633 vector was introduced into *Agrobacterium* strain AGL-1 and screened. cv. 'Fielder' and C-306 were transformed using *Agrobacterium*-mediated transformation, as described by (Bhati et al., 2016; Hayta *et al.*, 2021). Hygromycin was used to transform calli at 15mg/L in the first round, 30 mg/L in the second, and 20 mg/L during regeneration.

The presence of the transgene in regenerated plants was confirmed by PCR analysis using multiple pairs of Hygromycin cassette-specific primers, following the methodology of (Bhati *et al.*, 2016). Genomic DNA was extracted using the DNeasy Plant Pro Kit (Qiagen, Hilden, Germany) from pooled leaf discs collected from plants carrying the same constructs, following the manufacturer's protocol with the exception of using double the volume of grinding buffer. Target regions were amplified using conserved primers (**Table S1**) and GoTaq DNA Polymerase (Promega, USA) according to the manufacturer's instructions. A ~350 bp amplicon was generated from genomic DNA extracted from the edited lines. Firstly, these amplicons were subjected to the T7 Endonuclease *I* (T7E1) assay as described earlier (Kim *et al.*, 2014). To verify the occurrence of a DNA double-strand break, PCR amplicons were purified from agarose gel, denatured, reannealed, and subsequently T7EI assay was performed. The amplicons showing fragmentation were subjected to next-generation sequencing (Eurofins, Bangalaore, India). Mutagenesis in specific genomic regions was confirmed using Integrative Genomics Viewer (IGV) (Thorvaldsdóttir *et al.*, 2013). Additionally, Sanger sequencing (Eurofins Scientific DNA Sequencing Core) of the independently cloned PCR fragments was conducted to validate the nature of the edits as reflected in NGS data. Resulting sequences were analysed using the Synthego ICE Analysis

tool, which compares mutant sequences against the wild-type reference to determine editing efficiency or knockout scores.

Assessment of Root Architecture and Morphological Traits

Physiological and morphological traits, including plant height, number of grains per line, and 1000-grain weight, were recorded at the maturity stage (T_1 seeds). Each trait was evaluated using a minimum of three biological replicates from both transgenic edited lines and control plants.

Yeast-two-hybrid assays

Following PCR amplification, the complete coding sequences of *TaHRZ*1 and *TaHRZ*2 was cloned into the GAL4 activation domain vector pGADT7 (prey) and the GAL4 DNA-binding domain vector pGBKT7 (bait), respectively. The lithium acetate/PEG technique was used to co-transform the yeast strain AH109 (Clontech Matchmaker Gold System, USA) with bait and prey constructions in accordance with the manufacturer's instructions. The presence of both plasmids was verified by selecting transformants on synthetic dropout (SD) medium deficient in leucine and tryptophan (SD/-Leu/-Trp). Overnight growth of single colonies from SD/-Leu/-Trp plates was conducted at 30°C and 200 rpm in SD/-Leu/-Trp liquid medium. Serial 10-fold dilutions from 10□ to 10□³ were made in sterile distilled water after cultures were adjusted to an OD□□□ of 1.0. The yeast cultures were spotted (5 μL each) onto SD/-Leu/-Trp/-His + X-α-GAL plates in serial 10-fold dilutions from 10□ to 10□³ and incubated for 3–5 days at 30°C. The development of the blue colour and yeast growth were used to evaluate protein–protein interactions.

Statistical analysis

Statistical analyses were performed using one-way ANOVA or Student’s t-test with the SPSS software package (version 13.0, Windows). Data are expressed as mean ± standard error (SE) based on a minimum of three biological replicates.

Acknowledgements

The authors thank the Executive Director of NABI for facilities and support. The NABI-CORE grant to AKP supported this work. DBT-eLibrary Consortium (DeLCON) is acknowledged for providing timely support and access to e-resources for this work.

Contributions

Conceptualisation: DT and AKP; Project administration: AKP; Investigation: DT, AK, HB, KA, RJ, TL, VM,; Formal analyses: DT, AKP, VM; Visualization: DT, SBS, VM; Resources: AKP, KA, AK; Methodology: All authors. Supervision: AKP, AK. Writing-Original draft: AKP, DT; Writing- Review and Editing: AKP, TL, DT, SBS, VM, AK; Funding Acquisition: AKP.

Conflict of interest

The authors declare that they have no known competing financial interests or personal relationships that could have appeared to influence the work reported in this manuscript.

References:

Aggarwal, S., Kumar, A., Bhati, K.K., Kaur, G., Shukla, V., Tiwari, S., and Pandey, A.K. (2018) *RNAi-mediated downregulation of inositol pentakisphosphate kinase (IPK1) in wheat grains decreases phytic acid levels and increases Fe and Zn accumulation*. *Front Plant Sci*, **9**, 259.

Bailey, T.L., Johnson, J., Grant, C.E., and Noble, W.S. (2015) *The MEME suite*. *Nucleic Acids Res*, **43**, W39–W49.

Barberon, M., Zelazny, E., Robert, S., Conéjéro, G., Curie, C., Friml, J., and Vert, G. (2011) *Monoubiquitin-dependent endocytosis of the iron-regulated transporter 1 (IRT1) transporter controls iron uptake in plants*. *Proceedings of the National Academy of Sciences*, **108**, E450–E458.

Bauer, P., Ling, H.-Q., and Guerinot, M. Lou (2007) *FIT, the FER-like iron deficiency induced transcription factor in Arabidopsis*. *Plant Physiology and Biochemistry*, **45**, 260–261.

Bhati, K.K., Alok, A., Kumar, A., Kaur, J., Tiwari, S., and Pandey, A.K. (2016a) *Silencing of ABCC13 transporter in wheat reveals its involvement in grain development, phytic acid accumulation and lateral root formation*. *J Exp Bot*, **67**, 4379–4389.

Colangelo, E.P. and Guerinot, M. Lou (2004) *The essential basic helix-loop-helix protein FIT1 is required for the iron deficiency response*. *Plant Cell*, **16**, 3400–3412.

Connolly, E.L., Fett, J.P., and Guerinot, M. Lou (2002) *Expression of the IRT1 metal transporter is controlled by metals at the levels of transcript and protein accumulation*. *Plant Cell*, **14**, 1347–1357.

Curie, C., Cassin, G., Couch, D., Divol, F., Higuchi, K., Le Jean, M., et al. (2009) *Metal movement within the plant: contribution of nicotianamine and yellow stripe 1-like transporters*. *Ann Bot*, **103**, 1–11.

Curie, C., Panaviene, Z., Loulergue, C., Dellaporta, S.L., Briat, J.-F., and Walker, E.L. (2001) *Maize yellow stripe1 encodes a membrane protein directly involved in Fe (III) uptake*. *Nature*, **409**, 346–349.

Debernardi, J.M., Tricoli, D.M., Ercoli, M.F., Hayta, S., Ronald, P., Palatnik, J.F., and Dubcovsky, J. (2020) *A GRF–GIF chimeric protein improves the regeneration efficiency of transgenic plants*. *Nat Biotechnol*, **38**, 1274–1279.

Dubeaux, G., Neveu, J., Zelazny, E., and Vert, G. (2018) *Metal sensing by the IRT1 transporter-receptor orchestrates its own degradation and plant metal nutrition*. *Mol Cell*, **69**, 953–964.

Durrett, T.P., Gassmann, W., and Rogers, E.E. (2007) *The FRD3-mediated efflux of citrate into the root vasculature is necessary for efficient iron translocation*. *Plant Physiol*, **144**, 197–205.

Edgar, R.C. (2004) *MUSCLE: multiple sequence alignment with high accuracy and high throughput*. *Nucleic Acids Res*, **32**, 1792–1797.

Eide, D., Broderius, M., Fett, J., and Guerinot, M. Lou (1996) *A novel iron-regulated metal transporter from plants identified by functional expression in yeast. Proceedings of the National Academy of Sciences*, **93**, 5624–5628.

Filiz, E. and Kurt, F. (2019) *FIT (Fer-like iron deficiency-induced transcription factor) in plant iron homeostasis: genome-wide identification and bioinformatics analyses*. *J Plant Biochem Biotechnol*, **28**, 143–157.

Gao, F., Robe, K., Bettembourg, M., Navarro, N., Rofidal, V., Santoni, V., et al. (2020) *The transcription factor bHLH121 interacts with bHLH105 (ILR3) and its closest homologs to regulate iron homeostasis in Arabidopsis*. *Plant Cell*, **32**, 508–524.

Garbus, I., Romero, J.R., Valarik, M., Vanžurová, H., Karafiátová, M., Cáccamo, M., et al. (2015) *Characterization of repetitive DNA landscape in wheat homeologous group 4 chromosomes*. *BMC Genomics*, **16**, 1–16.

Hayta, S., Smedley, M.A., Clarke, M., Forner, M., and Harwood, W.A. (2021) *An efficient Agrobacterium mediated transformation protocol for hexaploid and tetraploid wheat*. *Curr Protoc*, **1**, e58.

Hindt, Maria N., Akmakjian, G.Z., Pivarski, K.L., Punshon, T., Baxter, I., Salt, D.E., and Guerinot, M. Lou (2017) *BRUTUS and its paralogs, BTS LIKE1 and BTS LIKE2, encode important negative regulators of the iron deficiency response in Arabidopsis thaliana*. *Metallomics*, **9**, 876–890.

Hindt, Maria N, Akmakjian, G.Z., Pivarski, K.L., Punshon, T., Baxter, I., Salt, D.E., and Guerinot, M. Lou (2017) *BRUTUS and its paralogs, BTS LIKE1 and BTS LIKE2, encode important negative regulators of the iron deficiency response in Arabidopsis thaliana*. *Metallomics*, **9**, 876–890.

Hu, B., Jin, J., Guo, A.-Y., Zhang, H., Luo, J., and Gao, G. (2015) *GSDS 2.0: an upgraded gene feature visualization server*. *Bioinformatics*, **31**, 1296–1297.

Iwase, A., Harashima, H., Ikeuchi, M., Rymen, B., Ohnuma, M., Komaki, S., et al. (2017) *WIND1 promotes shoot regeneration through transcriptional activation of ENHANCER OF SHOOT REGENERATION1 in Arabidopsis*. *Plant Cell*, **29**, 54–69.

Kaur, G., Shukla, V., Kumar, A., Kaur, M., Goel, P., Singh, P., et al. (2019) *Integrative analysis of hexaploid wheat roots identifies signature components during iron starvation*. *J Exp Bot*, **70**, 6141–6161.

Kim, Y.-H., Ramakrishna, S., Kim, H., and Kim, J.-S. (2014) *Enrichment of cells with TALEN-induced mutations using surrogate reporters*. *Methods*, **69**, 108–117.

Kobayashi, T., Nagasaka, S., Senoura, T., Itai, R.N., Nakanishi, H., and Nishizawa, Naoko K. (2013) *Iron-binding haemerythrin RING ubiquitin ligases regulate plant iron responses and accumulation*. *Nat Commun*, **4** 2792.

Kobayashi, T. and Nishizawa, N.K. (2012) *Iron uptake, translocation, and regulation in higher plants*. *Annu Rev Plant Biol*, **63**, 131–152.

Kobayashi, T., Ozu, A., Kobayashi, S., An, G., Jeon, J.-S., and Nishizawa, N.K. (2019) *OsbHLH058 and OsbHLH059 transcription factors positively regulate iron deficiency responses in rice*. *Plant Mol Biol*, **101**, 471–486.

Kumar, A., Kaur, G., Singh, P., Meena, V., Sharma, S., Tiwari, M., et al. (2022) *Strategies and bottlenecks in hexaploid wheat to mobilize soil iron to grains*. *Front Plant Sci*, **13**, 863849.

Kumar, S., Stecher, G., Li, M., Knyaz, C., and Tamura, K. (2018) *MEGA X: molecular evolutionary genetics analysis across computing platforms*. *Mol Biol Evol*, **35**, 1547–1549.

Laux, T., Mayer, K.F.X., Berger, J., and Jürgens, G. (1996) *The WUSCHEL gene is required for shoot and floral meristem integrity in Arabidopsis*. *Development*, **122**, 87–96.

Li, M., Watanabe, S., Gao, F., and Dubos, C. (2023) *Iron nutrition in plants: towards a new paradigm? Plants 12: 384*.

Li, Y., Lu, C.K., Li, C.Y., Lei, R.H., Pu, M.N., Zhao, J.H., et al. (2021) *IRON MAN interacts with BRUTUS to maintain iron homeostasis in Arabidopsis*. *Proceedings of the National Academy of Sciences*, **118**, e2109063118.

Livak, K.J. and Schmittgen, T.D. (2001) *Analysis of relative gene expression data using real-time quantitative PCR and the 2− ΔΔCT method*. *methods*, **25**, 402–408.

Long, T.A., Tsukagoshi, H., Busch, W., Lahner, B., Salt, D.E., and Benfey, P.N. (2010) *The bHLH transcription factor POPEYE regulates response to iron deficiency in Arabidopsis roots*. *Plant Cell*, **22**, 2219–2236.

Lowe, K., La Rota, M., Hoerster, G., Hastings, C., Wang, N., Chamberlin, M., et al. (2018) *Rapid genotype "independent" Zea mays L.(maize) transformation via direct somatic embryogenesis*. *In Vitro Cellular & Developmental Biology-Plant*, **54**, 240–252.

Ofori, K.F., Antoniello, S., English, M.M., and Aryee, A.N.A. (2022) *Improving nutrition through biofortification–A systematic review*. *Front Nutr*, **9**, 1043655.

Pal, V., Singh, G., and Dhaliwal, S.S. (2021) *A new approach in agronomic biofortification for improving zinc and iron content in chickpea (Cicer arietinum L.) grain with simultaneous foliar application of zinc sulphate, ferrous sulphate and urea*. *J Soil Sci Plant Nutr*, **21**, 883–896.

Palmer, C.M. and Guerinot, M. Lou (2009) *Facing the challenges of Cu, Fe and Zn homeostasis in plants*. *Nat Chem Biol*, **5**, 333–340.

Pullin, J., Rodríguez-Celma, J., Franceschetti, M., Mundy, J.E.A., Svistunenko, D.A., Bradley, J.M., et al. (2025) *Iron-sensing and redox properties of the hemerythrin-like domains of Arabidopsis BRUTUS and BRUTUS-LIKE2 proteins*. *Nat Commun*, **16**, 3865.

Robinson, N.J., Procter, C.M., Connolly, E.L., and Guerinot, M. Lou (1999) *A ferric-chelate reductase for iron uptake from soils*. *Nature*, **397**, 694–697.
Rodríguez-Celma, J., Connorton, J.M., Kruse, I., Green, R.T., Franceschetti, M., Chen, Y.-T., et al. (2019) *Arabidopsis BRUTUS-LIKE E3 ligases negatively regulate iron uptake by targeting transcription factor FIT for recycling*. *Proceedings of the National Academy of Sciences*, **116**, 17584–17591.
Salahudeen, A.A., Thompson, J.W., Ruiz, J.C., Ma, H.-W., Kinch, L.N., Li, Q., et al. (2009) *An E3 ligase possessing an iron-responsive hemerythrin domain is a regulator of iron homeostasis*. *Science (1979)*, **326**, 722–726.
Santi, S. and Schmidt, W. (2009) *Dissecting iron deficiency induced proton extrusion in Arabidopsis roots*. *New Phytologist*, **183**, 1072–1084.
Selote, D., Samira, R., Matthiadis, A., Gillikin, Jeffrey W., and Long, T.A. (2015) *Iron-binding e3 ligase mediates iron response in plants by targeting basic helix-loop-helix transcription factors1[open]*. *Plant Physiol*, **167**, 273–286.
Shin, L.-J., Lo, J.-C., Chen, G.-H., Callis, J., Fu, H., and Yeh, K.-C. (2013) *IRT1 degradation factor1, a ring E3 ubiquitin ligase, regulates the degradation of iron-regulated transporter1 in Arabidopsis*. *Plant Cell*, **25**, 3039–3051.
Sperotto, R.A., Ricachenevsky, F.K., de Abreu Waldow, V., and Fett, J.P. (2012) *Iron biofortification in rice: it's a long way to the top*. *Plant Science*, **190**, 24–39.
Spielmann, J. and Vert, G. (2021) *The many facets of protein ubiquitination and degradation in plant root iron-deficiency responses*. *J Exp Bot*, **72**, 2071–2082.
Thorvaldsdóttir, H., Robinson, J.T., and Mesirov, J.P. (2013) *Integrative Genomics Viewer (IGV): high-performance genomics data visualization and exploration*. *Brief Bioinform*, **14**, 178–192.
Vashisht, A.A., Zumbrennen, K.B., Huang, X., Powers, D.N., Durazo, A., Sun, D., et al. (2009) *Control of iron homeostasis by an iron-regulated ubiquitin ligase*. *Science (1979)*, **326**, 718–721.
Vert, G., Grotz, N., Dédaldéchamp, F., Gaymard, F., Guerinot, M. Lou, Briat, J.-F., and Curie, C. (2002) *IRT1, an Arabidopsis transporter essential for iron uptake from the soil and for plant growth*. *Plant Cell*, **14**, 1223–1233.
Wulff, B.B.H. and Dhugga, K.S. (2018) *Wheat—the cereal abandoned by GM*. *Science (1979)*, **361**, 451–452.
Yuan, Y., Wu, H., Wang, N., Li, J., Zhao, W., Du, J., et al. (2008) *FIT interacts with AtbHLH38 and AtbHLH39 in regulating iron uptake gene expression for iron homeostasis in Arabidopsis*. *Cell Res*, **18**, 385–397.
Zaman, Q.U., Li, C., Cheng, H., and Hu, Q. (2019) *Genome editing opens a new era of genetic improvement in polyploid crops*. *Crop J*, **7**, 141–150.
Zhang, X., Henriques, R., Lin, S.-S., Niu, Q.-W., and Chua, N.-H. (2006) *Agrobacterium-mediated transformation of Arabidopsis thaliana using the floral dip method*. *Nat Protoc*, **1**, 641–646.

Legends for Figures:

Figure 1: Phylogeny and characterization of Wheat HRZ1 and HRZ2 proteins**.** (A) Schematic representation of the wheat HRZ protein domains. Both proteins contain three

Hemerythrin (HHE) domains and a single zf-CHY, RING-UB domain with Zinc ribbon motifs. (B) Phylogenetic analysis of *TaHRZ*1 and *TaHRZ*2 homoeologs and other known HRZ proteins from *Arabidopsis* (At), *Zea mays* (Zm), *Brachypodium* (Bd) and rice (Os) homologs grouped them into 1st and 2nd clade main clades. The MUSCLE algorithm was used to align MCO proteins, and the MEGA 11 neighbour-joining method was used to create an unrooted phylogenetic tree with a bootstrap value of 1000. (C) In-silico expVIP expression analysis of *TaHRZ* gene homoeologs in different wheat tissues at different phases of wheat development.

Figure 2: Relative expression analysis of *TaHRZ*1 and *TaHRZ*2 in wheat roots and shoots under Fe deficiency conditions. (A) Relative expression of *TaHRZ*1 and (B) *TaHRZ*2 at 4D and 8D Fe resupply treatment. Fe was supplied as Fe-EDTA, at 80µM Fe-EDTA (+Fe) and 1µM Fe-EDTA (–Fe). (C) *TaHRZ*1*/HRZ*2 expression in wheat plants varies by different developmental stages. The analysis was occurred at four different developmental stages: 7, 14, 21, and 28 days after anthesis (DAA). (D) Quantitative Expression Analysis of *TaHRZ1/HRZ*2 in several tissues inside the grain, including the p:pericarp; al:aleurone; em:embryo; en:endosperm. To normalize the expression level, TaARF1 was used as an internal reference gene. Fold change were determined using the 2^−ΔΔCT method in all the panels. The standard deviation was calculated from three biological replicates (n=3). Significant difference ($P < 0.05$) were shown by different letters above the bars using one way Anova analysis.

Figure 3: Genetic complementation of *atbts*1 with *TaHRZ*1 and *TaHRZ*2 and its characterization. (A) Phenotypic analysis of *TaHRZ*1 and *TaHRZ*2 complemented lines (Ox-L1 and Ox-L2) in atbts1 mutant (bts1) along with Col-0 (WT). Plants were grown on Hoagland solid medium for 5 days, then transferred to –Fe (200 µM Ferrozine) media for 1 weeks. Under iron deficiency bts1 mutant exhibits long root growth compared to Col-0.

Arabidopsis complementing line *TaHRZ1/HRZ2* reversed the mutant phenotype, resulting in reduced primary root length growth in iron deficiency. (B) Estimation of the total chlorophyll content in the leaves of the treated plants. Chlorophyll assessment was performed using 100mg of leaf tissue. The atbts1 mutant shown markedly significant increase in the chlorophyll contents under -Fe, +Fe, compared to Col-0 and complementing lines. (C) Total Fe was measured in the seedlings using ICP-MS analysis. (D) Representative images of Fe distribution in Col-0, bts1, ox-L1 (HRZ1) and ox-L2 (HRZ2) and *TaHRZ* complementaion Arabidopsis lines, detected by Perls staining. Under +Fe, –Fe condition Col-0, *TaHRZ* complementing lines showed less iron accumulation as compared to atbts1. (E) Fe chelate reductase activity of wheat roots (n=30) in the lines. Letters above the bars indicate significant differences ($P < 0.05$) between genotypes, as determined by a two-way ANOVA test.

Figure 4: Yeast two-hybrid interactions of TaHRZ1 and TaHRZ2 with the target proteins**.** (A) Western confirmation of the expression of TaHRZ1 and TaHRZ2 proteins fused with c-Myc in the yeast strain subjected to Y2H assays. (B) Spot growth assay of Y2H GOLD strains expressing a combination of BD- *TaHRZ*1 with AD-BHLH, FIT, BD-*TaHRZ*2 with AD-BHLH, FIT. Positive and negative control interaction were also included. (C) Western analysis of the truncated wheat HRZ proteins (t-HRZ) and their interaction of t-*TaHRZ*1 and t-*TaHRZ*2 with *TabHLH* IVc and *TaFIT*. Dilutions of OD_{600}= 0.100, 0.010, 0.001 and 0.0001 were spotted on solid SC medium or solid SC medium with -LTHA. Plates were incubated at 30 °C for 3 days to assess growth and reporter activity

Figure 5: CRISPR-Cas9 mediating editing of HHE3 in TaHRZ1**.** (A) CRISPR-CAS9 editing of HHE3 domain using GRF4-GIF1 to enhance wheat regeneration. HHE3 domain of *TaHRZ*1 was targeted by gRNA for genome editing**.** (B) The structure that carries the wheat GRF4-GIF1 chimeric protein was derived from JD633 (Addgene). The maize Ubi promoter

drives the Cas9 expression, and the gRNA expression is driven by the TaU6 promoter. (C) Comparison of post-transformation tissue culture stage in wheat using different constructs. Regeneration response compared to the empty vector (pRGEB32) and GRF4-GIF1 derived clone, across the tissue culture stages. (D) Phenotype of ed-hrz1 in cv. C306 and cv. Fielder. The pictures were taken post-45 days of growth at the T_1 generation stage. (E) Western blot analysis to confirm Cas9:*TaHRZ*1 protein expression in transgenic lines. Total protein was extracted from multiple transgenic lines and probed with anti-Cas9 as the primary antibody and anti-mouse as the secondary antibody. Three lines displayed distinct positive bands at ~151 kDa, confirming the successful expression of the Cas9:*TaHRZ*1 fusion protein. Phenotype of ed-hrz1 and ed-hrz2 (edited lines) in cvs. C306 and Fielder. The pictures were taken post 45 days of growth at T_1 generation stage.

Figure 6: CRISPR edits analysis from Sanger sequencing data of the targeted region near the PAM site to detect interference of CRISPR edits using Synthego. (A) Indel percentages were estimated using Sanger sequencing data, and R^2 values were used to assess the accuracy of editing. Sanger Chromatograms from CRISPR-edited wheat lines of Fielder (D1, D3, D7) and C306 (C3, C11) were analyzed for indel mutations at the target site. High R^2 values confirmed efficient and reliable genome editing in the selected lines. Editing efficiency scores of CRISPR-edited wheat lines (Fielder: D1, D3, D7; C306: C3, C11) were calculated based on indel frequencies using Sanger sequencing data. (B) Alignment of the expectations and the different edits containing the insertions and deletions at the target site. R^2 values represent the confidence in mutation detection and quantification. The red arrow indicates the PAM site (NGG) with the gRNA sequence.

Figure 7: Characterization of wheat CRISPR-Cas9 edits**.** (A) Phenotype of the grains from the edited lines of two cultivars (B) Representative images of Perl's Blue staining for transverse cross-sections of transgenic wheat grains (T_1) at grain maturation. (C) ICP-MS

analysis of mature wheat grains (T_1) (n=4; primary spike). (C) The molar ratios of Iron:Phytate (Fe:PA) were calculated for the mature wheat grains (T_1) (n=4; primary spike) generated from the transgenic lines and non-transgenic. (E) Average total grain number per plant (n=6). (F) Average total grain weight (1000 grain) in edited lines (GRF4-GIF1). (G) Plant height in cm. Data represent the mean ± SE of six *TaHRZ1* and at least six WT in Fielder, six *TaHRZ1* and six WT in the cv. C306. None of the traits showed any statistically significant differences between the gene-edited and non-transformed control plants. Letters above the bars indicate statistically significant differences ($P < 0.05$) between genotypes, as determined by one-way ANOVA.

Figure 8: Expression analysis of genes using qRT-PCR in control and edited lines**.** Relative expression of Fe homeostasis genes (A) *TaHRZ*1, (B) *TaHRZ*2, (C) *TaIDEF*1, (D) *TaIRO*3 and (E) *TaFIT* in edited (D1, D3, D7) and control lines (WT) under –Fe and +Fe conditions. Each bar indicates the mean of three replicates with the indicated standard deviation of the mean. C_t values were normalized using *TaARF1* as an internal control. Letters above the bars indicate statistically significant differences ($P < 0.05$) between genotypes, as determined by one-way ANOVA.

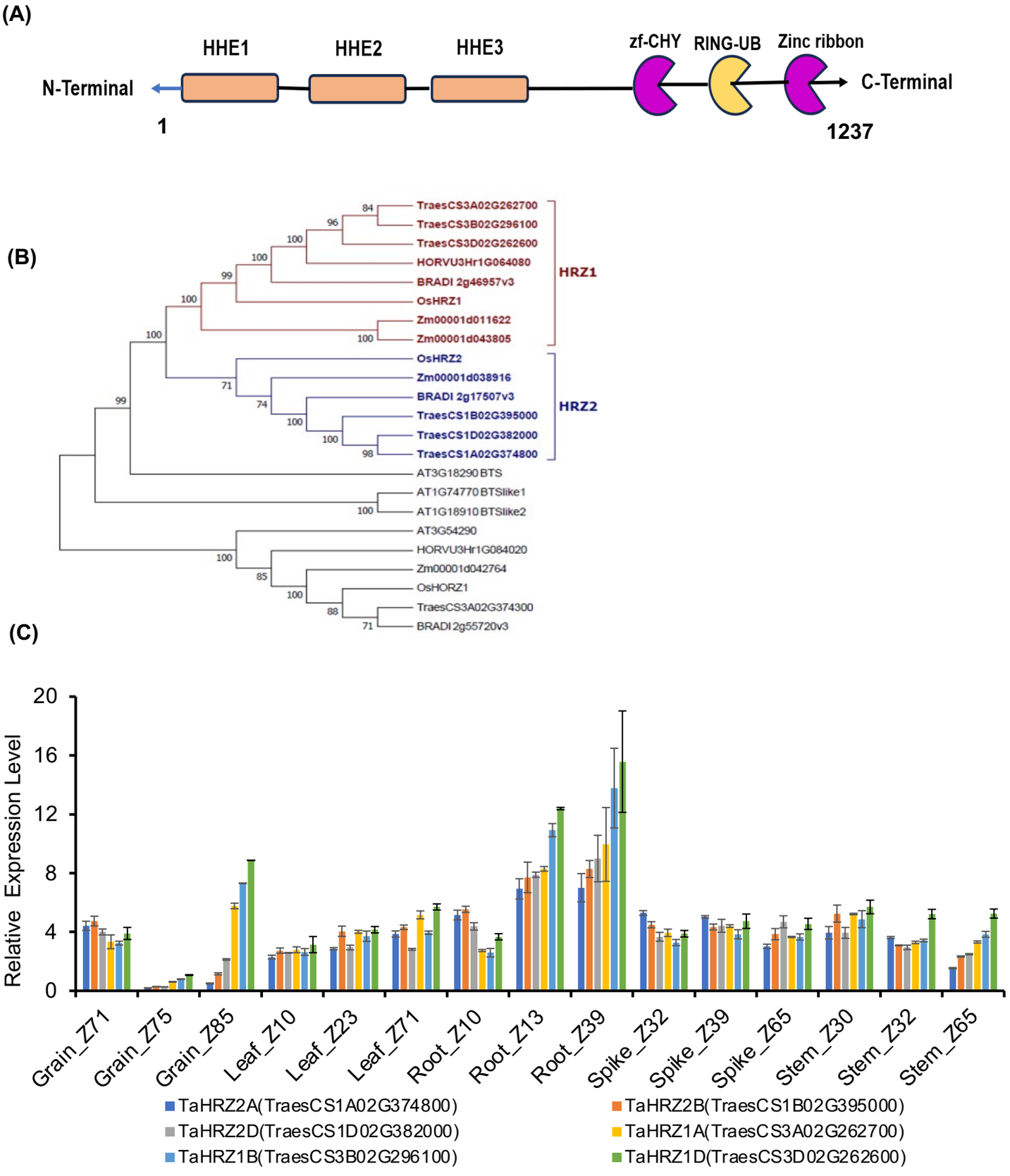
(A)
HHE1
HHE2
HHE3
zf-CHY
RING-UB
Zinc ribbon
N-Terminal
C-Terminal
1
1237
(B)
TraesCS3A02G262700
TraesCS3B02G296100
TraesCS3D02G262600
HORVU3Hr1G064080
BRADI 2g46957v3
OsHRZ1
Zm00001d011622
Zm00001d043805
HRZ1
OsHRZ2
Zm00001d038916
BRADI 2g17507v3
TraesCS1B02G395000
TraesCS1D02G382000
TraesCS1A02G374800
HRZ2
AT3G18290 BTS
AT1G74770 BTSlike1
AT1G18910 BTSlike2
AT3G54290
HORVU3Hr1G084020
Zm00001d042764
OsHORZ1
TraesCS3A02G374300
BRADI 2g55720v3
(C)
Relative Expression Level
0
4
8
12
16
20
Grain_Z71
Grain_Z75
Grain_Z85
Leaf_Z10
Leaf_Z23
Leaf_Z71
Root_Z10
Root_Z13
Root_Z39
Spike_Z32
Spike_Z39
Spike_Z65
Stem_Z30
Stem_Z32
Stem_Z65
TaHRZ2A(TraesCS1A02G374800)
TaHRZ2B(TraesCS1B02G395000)
TaHRZ2D(TraesCS1D02G382000)
TaHRZ1A(TraesCS3A02G262700)
TaHRZ1B(TraesCS3B02G296100)
TaHRZ1D(TraesCS3D02G262600)

Figure 1

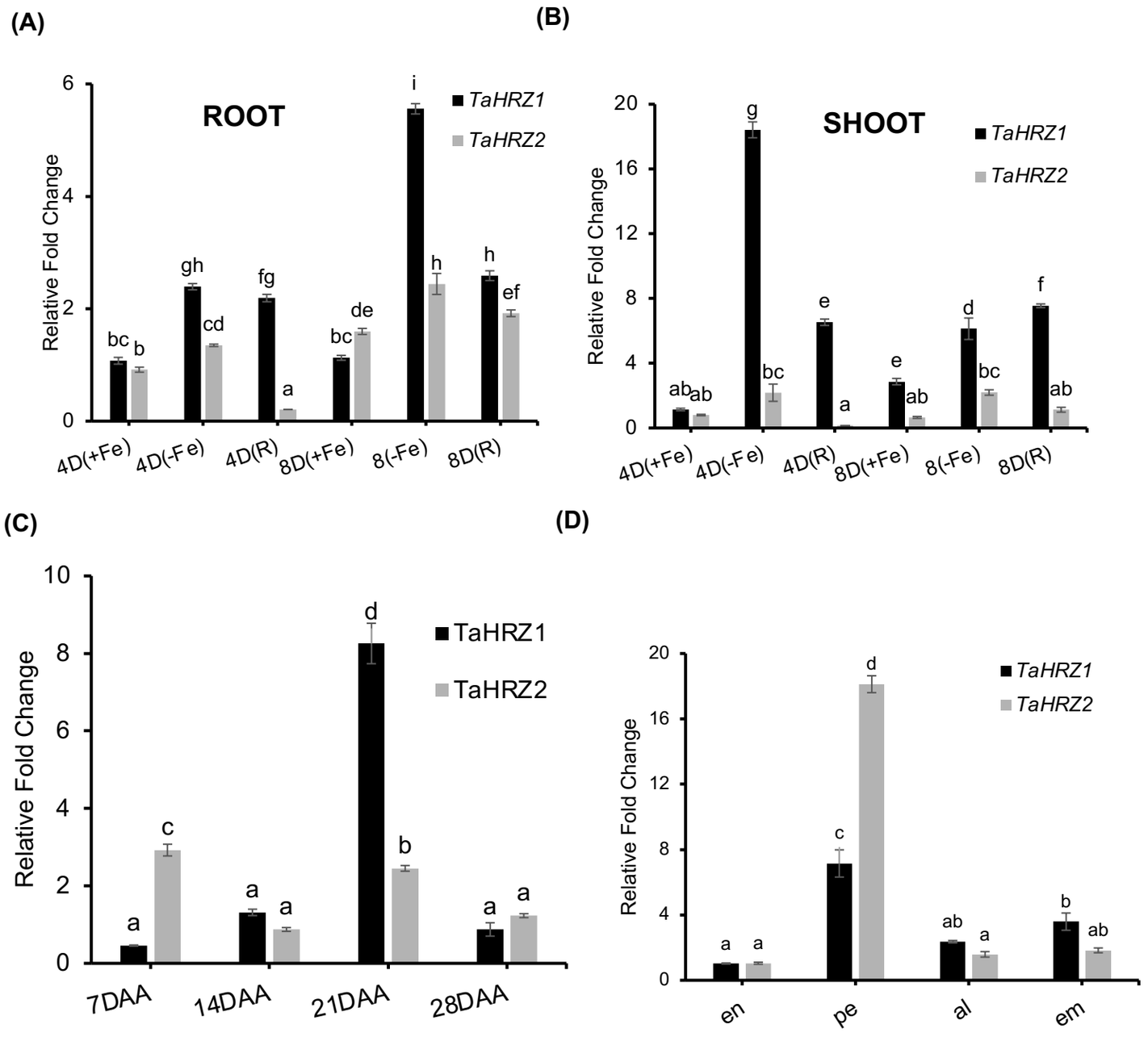
(A)
ROOT
TaHRZ1
TaHRZ2
Relative Fold Change
0
2
4
6
bc
b
gh
cd
fg
a
bc
de
i
h
h
ef
4D(+Fe)
4D(-Fe)
4D(R)
8D(+Fe)
8(-Fe)
8D(R)
(B)
SHOOT
TaHRZ1
TaHRZ2
Relative Fold Change
0
4
8
12
16
20
ab
ab
g
bc
e
a
e
ab
d
bc
f
ab
4D(+Fe)
4D(-Fe)
4D(R)
8D(+Fe)
8(-Fe)
8D(R)
(C)
TaHRZ1
TaHRZ2
Relative Fold Change
0
2
4
6
8
10
a
c
a
a
d
b
a
a
7DAA
14DAA
21DAA
28DAA
(D)
TaHRZ1
TaHRZ2
Relative Fold Change
0
4
8
12
16
20
a
a
c
d
ab
a
b
ab
en
pe
al
em

Figure 2

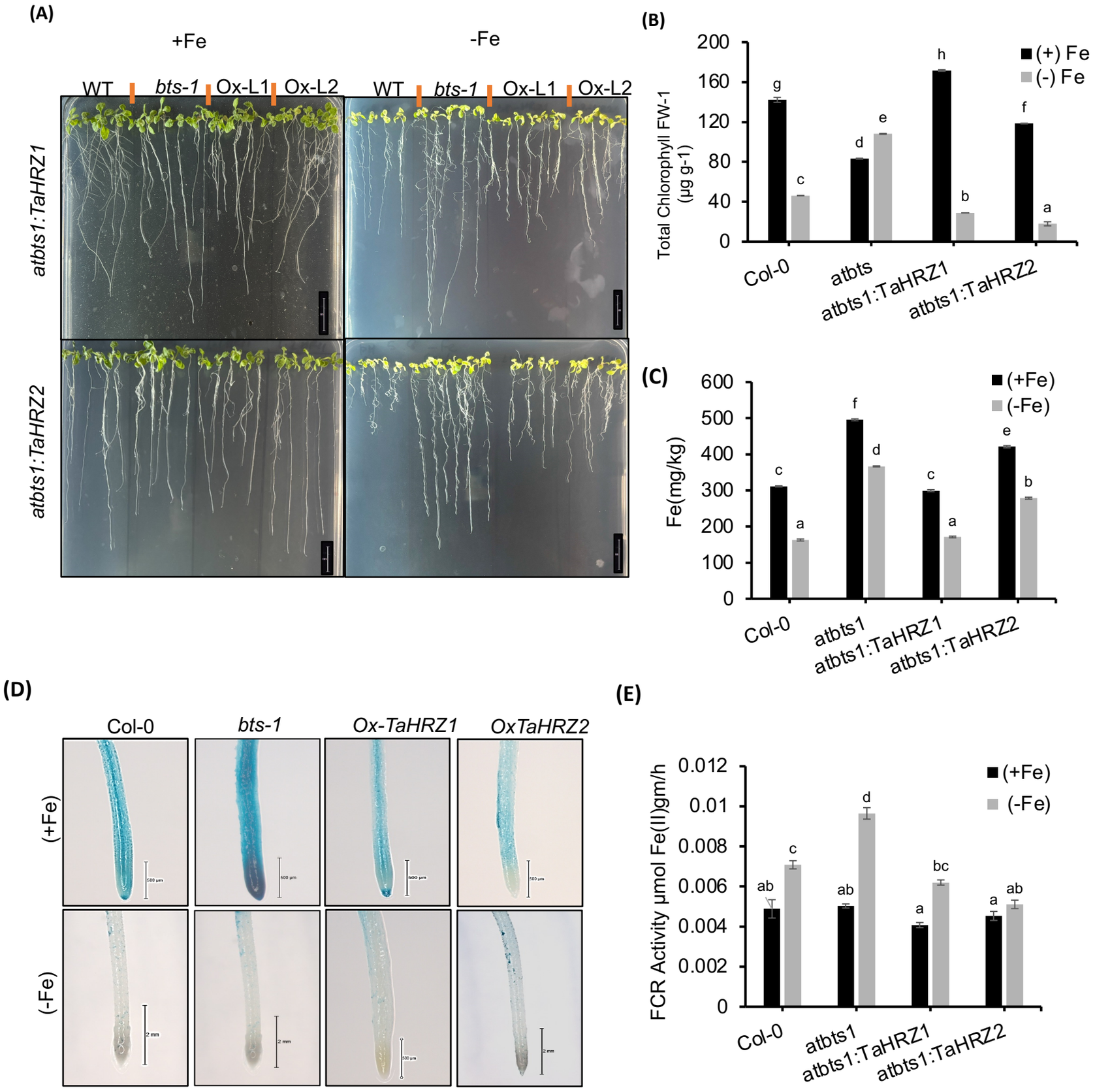
(A)
+Fe
-Fe
WT
bts-1
Ox-L1
Ox-L2
atbts1:TaHRZ1
atbts1:TaHRZ2
(B)
Total Chlorophyll FW-1 (µg g-1)
(+) Fe
(-) Fe
Col-0
atbts
atbts1:TaHRZ1
atbts1:TaHRZ2
(C)
Fe(mg/kg)
(+Fe)
(-Fe)
Col-0
atbts1
atbts1:TaHRZ1
atbts1:TaHRZ2
(D)
Col-0
bts-1
Ox-TaHRZ1
OxTaHRZ2
(+Fe)
(-Fe)
(E)
FCR Activity µmol Fe(II)gm/h
(+Fe)
(-Fe)
Col-0
atbts1
atbts1:TaHRZ1
atbts1:TaHRZ2

Figure 3

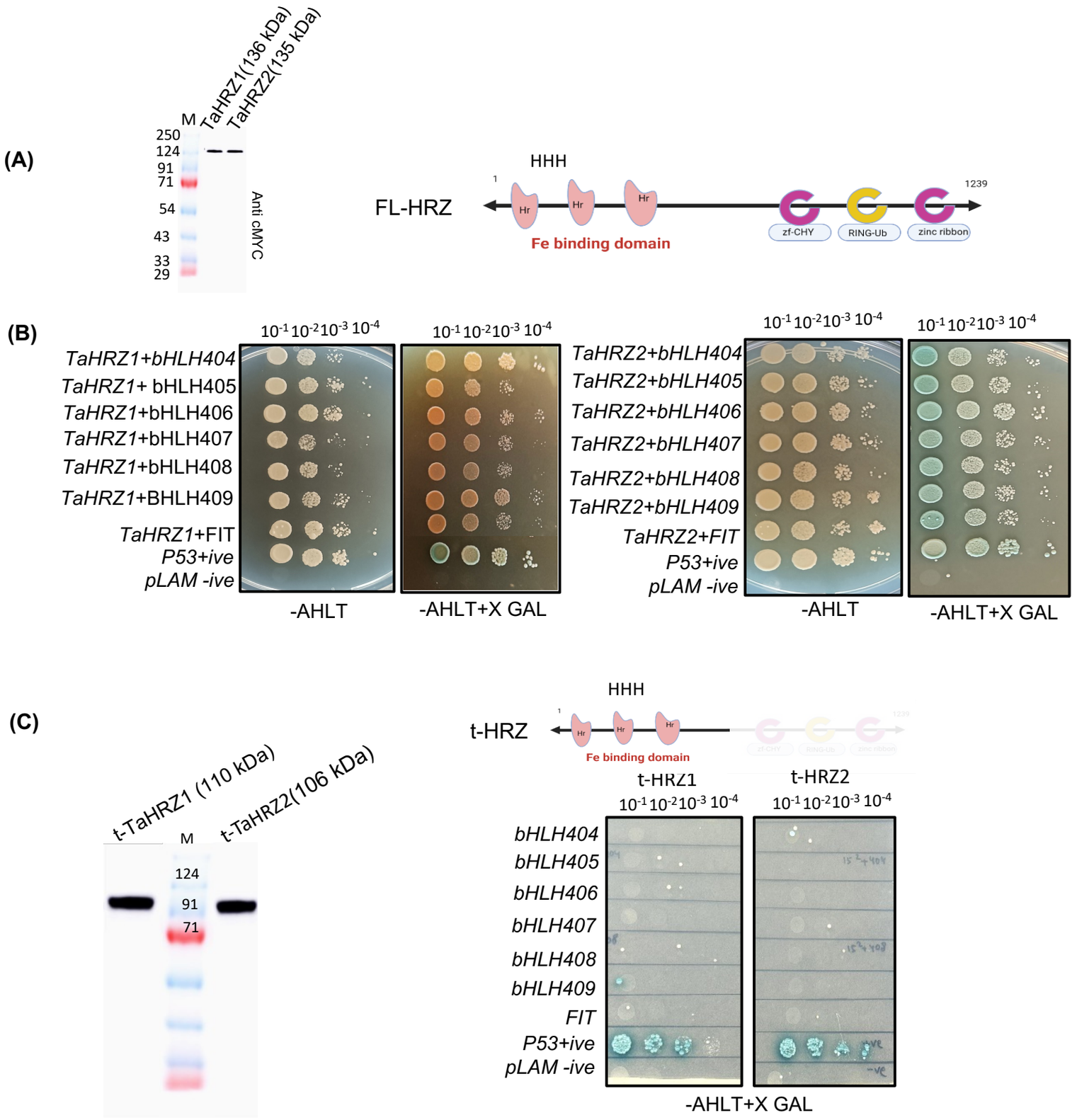
(A)
M
TaHRZ1(136 kDa)
TaHRZ2(135 kDa)
250
124
91
71
54
43
33
29
Anti cMYC
FL-HRZ
HHH
1
1239
Hr
Hr
Hr
Fe binding domain
zf-CHY
RING-Ub
zinc ribbon
(B)
10-1 10-2 10-3 10-4
TaHRZ1+bHLH404
TaHRZ1+ bHLH405
TaHRZ1+bHLH406
TaHRZ1+bHLH407
TaHRZ1+bHLH408
TaHRZ1+BHLH409
TaHRZ1+FIT
P53+ive
pLAM -ive
-AHLT
-AHLT+X GAL
TaHRZ2+bHLH404
TaHRZ2+bHLH405
TaHRZ2+bHLH406
TaHRZ2+bHLH407
TaHRZ2+bHLH408
TaHRZ2+bHLH409
TaHRZ2+FIT
P53+ive
pLAM -ive
(C)
t-TaHRZ1 (110 kDa)
M
t-TaHRZ2(106 kDa)
124
91
71
t-HRZ
HHH
Fe binding domain
t-HRZ1
t-HRZ2
10-1 10-2 10-3 10-4
bHLH404
bHLH405
bHLH406
bHLH407
bHLH408
bHLH409
FIT
P53+ive
pLAM -ive
-AHLT+X GAL

Figure 4

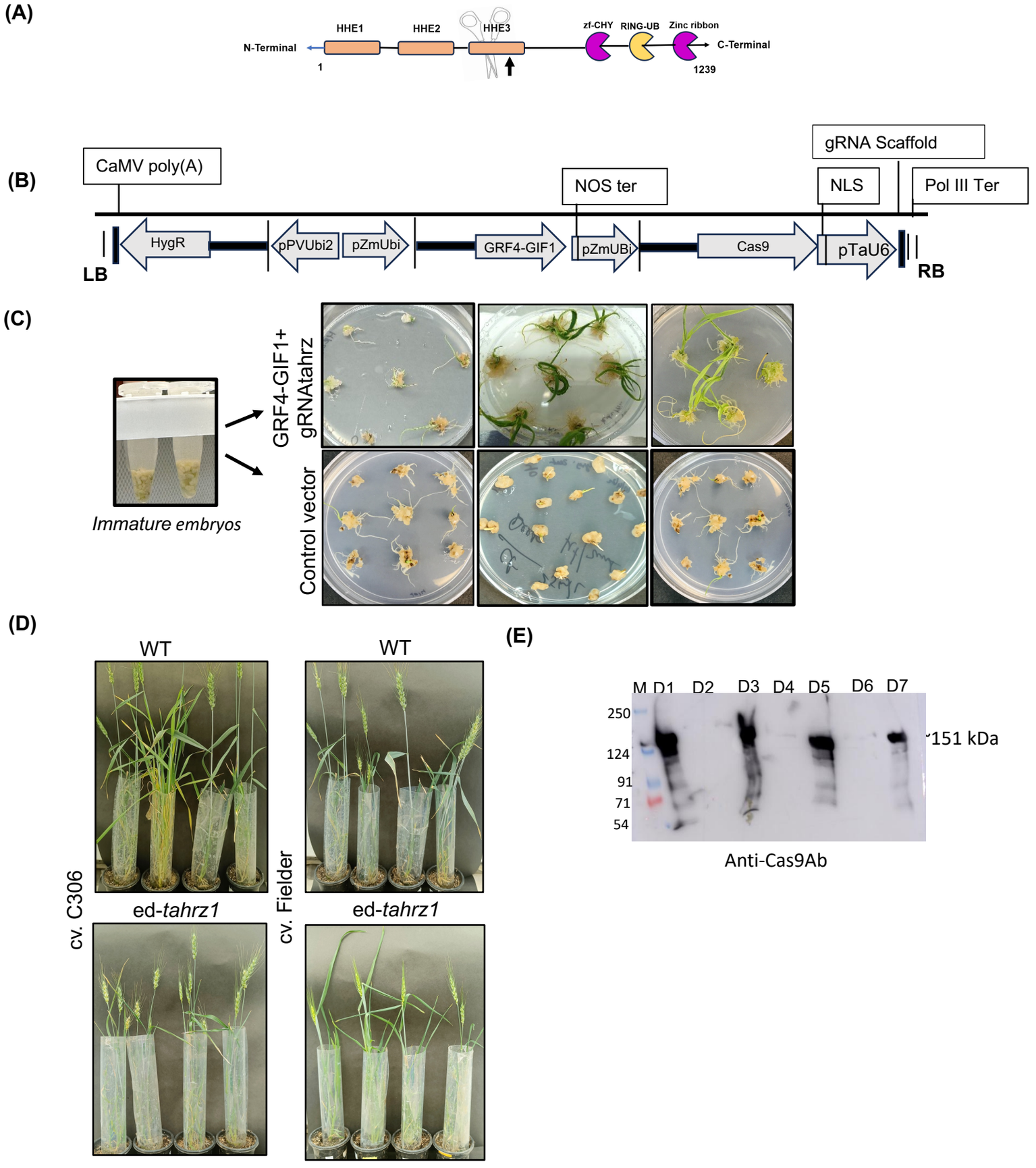
(A)
HHE1
HHE2
HHE3
zf-CHY
RING-UB
Zinc ribbon
N-Terminal
C-Terminal
1
1239
(B)
CaMV poly(A)
gRNA Scaffold
NOS ter
NLS
Pol III Ter
HygR
pPVUbi2
pZmUbi
GRF4-GIF1
pZmUBi
Cas9
pTaU6
LB
RB
(C)
Immature embryos
GRF4-GIF1+ gRNAtahrz
Control vector
(D)
WT
WT
ed-tahrz1
ed-tahrz1
cv. C306
cv. Fielder
(E)
M D1 D2 D3 D4 D5 D6 D7
250
124
91
71
54
~151 kDa
Anti-Cas9Ab

Figure 5

(A)

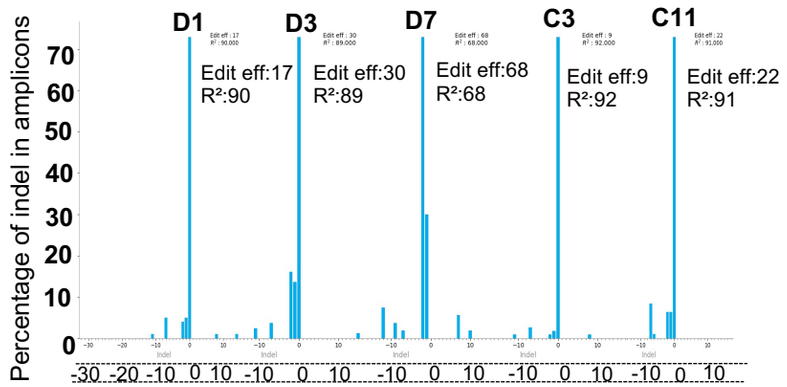
D1
D3
D7
C3
C11
Edit eff:17
R²:90
Edit eff:30
R²:89
Edit eff:68
R²:68
Edit eff:9
R²:92
Edit eff:22
R²:91
Percentage of indel in amplicons
70
60
50
40
30
20
10
0
-30 -20 -10 0 10 -10 0 10 -10 0 10 -10 0 10 -10 0 10

(B)

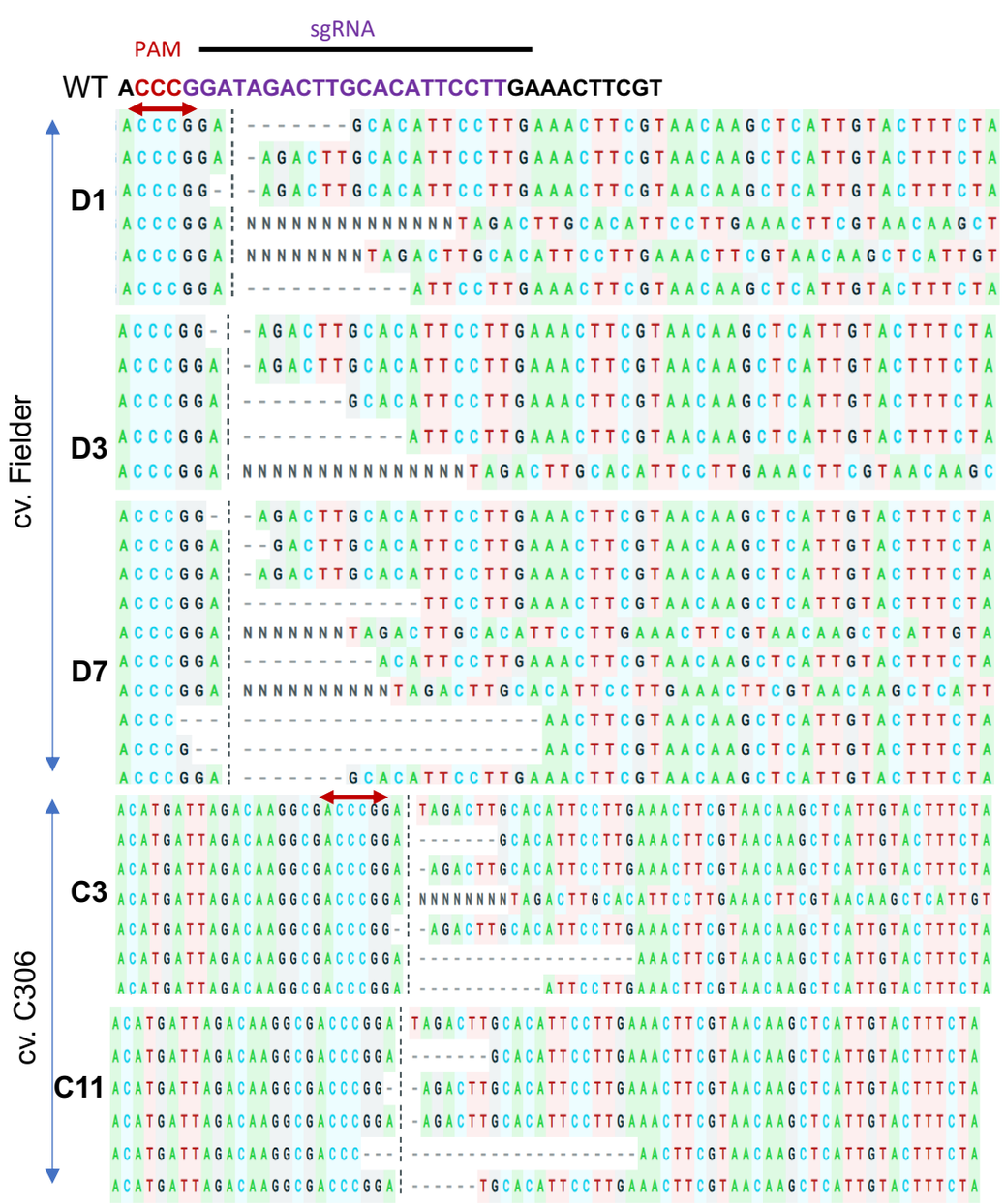
PAM
sgRNA
WT ACCCGGATAGACTTGCACATTCCTTGAAACTTCGT
cv. Fielder
D1
D3
D7
cv. C306
C3
C11

Figure 6

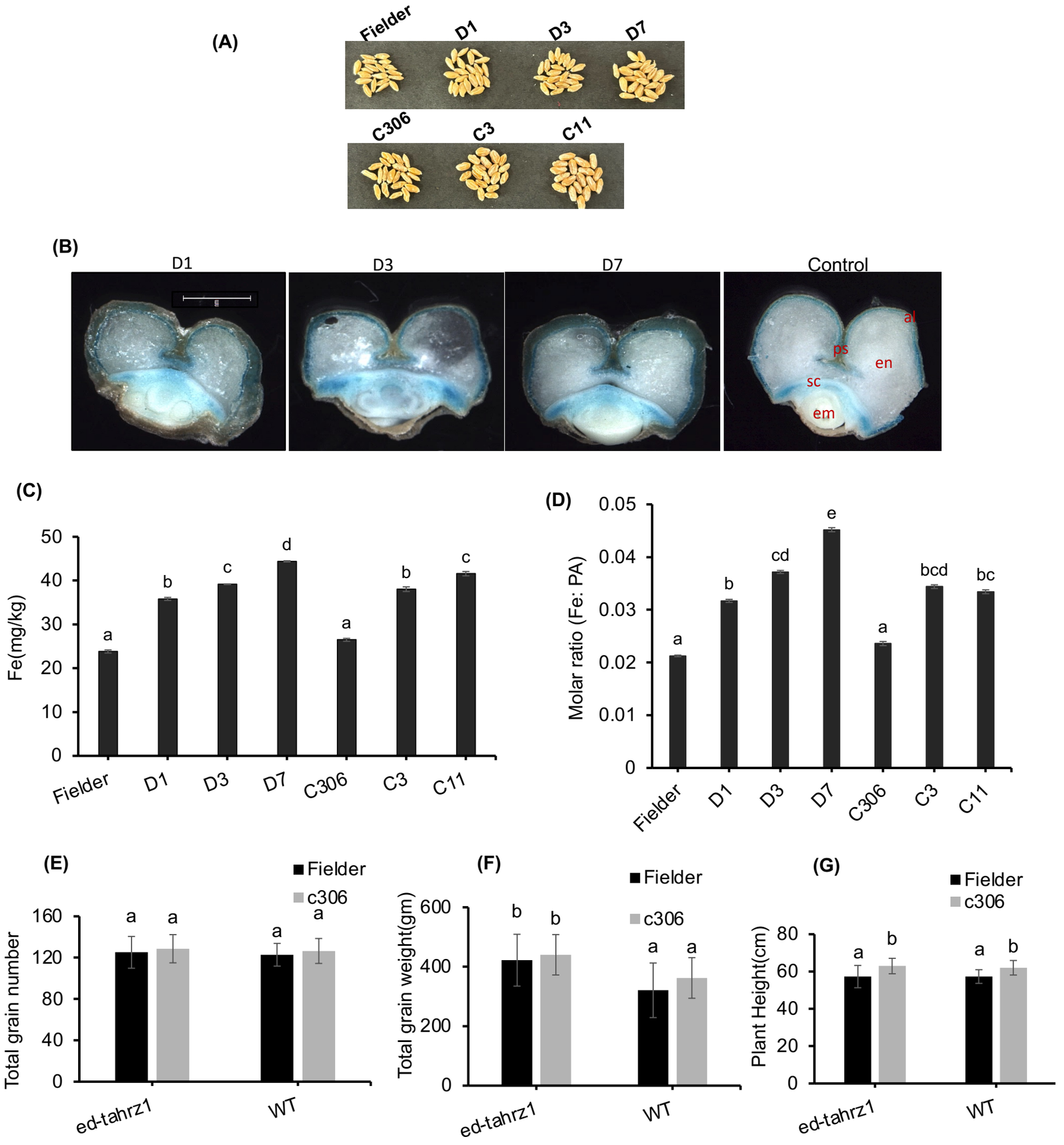
(A)
Fielder
D1
D3
D7
C306
C3
C11
(B)
D1
D3
D7
Control
al
ps
en
sc
em
(C)
Fe(mg/kg)
50
40
30
20
10
0
a
b
c
d
a
b
c
Fielder
D1
D3
D7
C306
C3
C11
(D)
Molar ratio (Fe: PA)
0.05
0.04
0.03
0.02
0.01
0
a
b
cd
e
a
bcd
bc
Fielder
D1
D3
D7
C306
C3
C11
(E)
Fielder
c306
Total grain number
160
120
80
40
0
a
a
a
a
ed-tahrz1
WT
(F)
Fielder
c306
Total grain weight(gm)
600
400
200
0
b
b
a
a
ed-tahrz1
WT
(G)
Fielder
c306
Plant Height(cm)
80
60
40
20
0
a
b
a
b
ed-tahrz1
WT

Figure 7

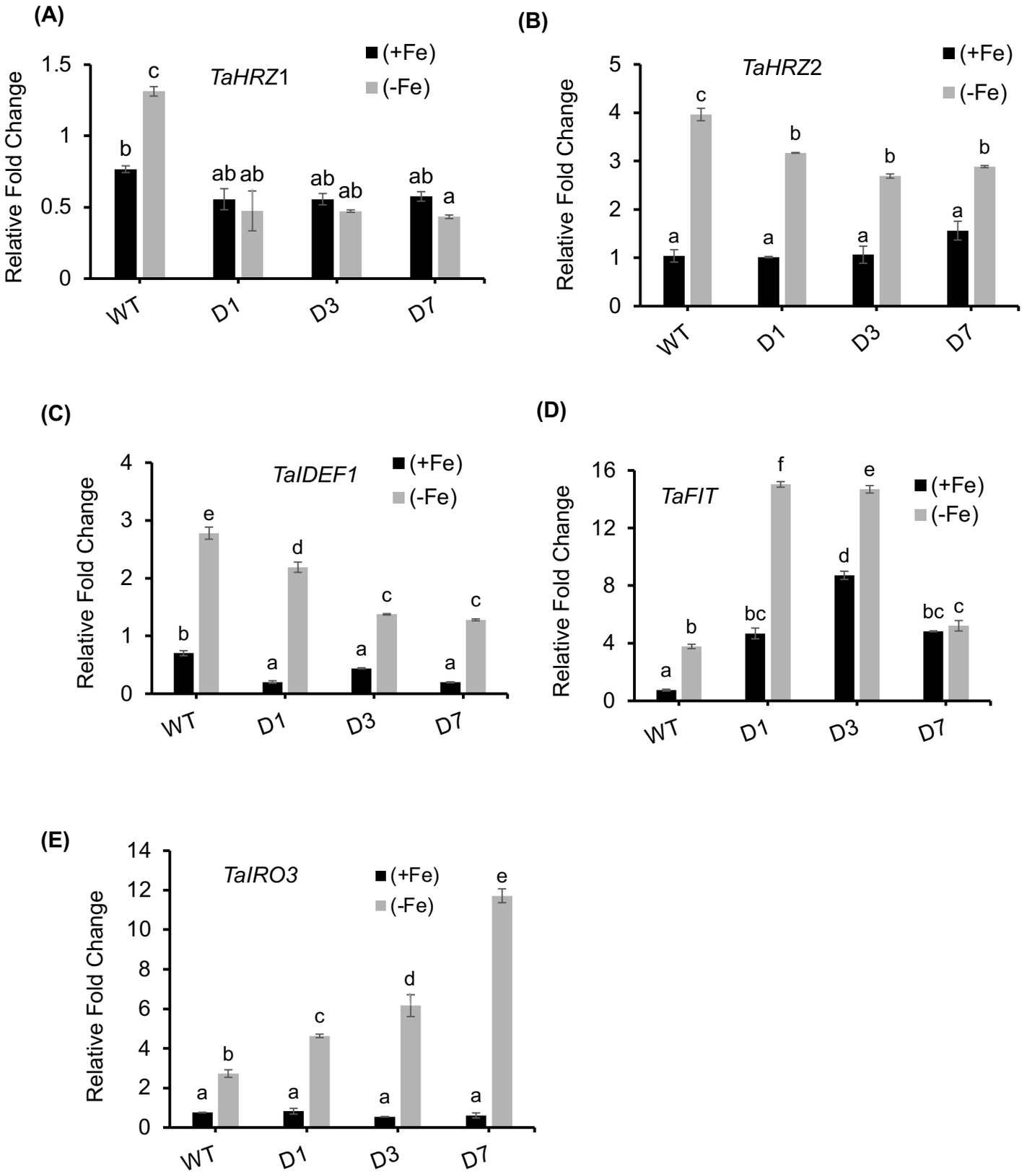
(A)
TaHRZ1
(+Fe)
(-Fe)
Relative Fold Change
1.5
1
0.5
0
b
c
ab
ab
ab
ab
ab
a
WT
D1
D3
D7
(B)
TaHRZ2
(+Fe)
(-Fe)
Relative Fold Change
5
4
3
2
1
0
a
c
a
b
a
b
a
b
WT
D1
D3
D7
(C)
TaIDEF1
(+Fe)
(-Fe)
Relative Fold Change
4
3
2
1
0
b
e
a
d
a
c
a
c
WT
D1
D3
D7
(D)
TaFIT
(+Fe)
(-Fe)
Relative Fold Change
16
12
8
4
0
a
b
bc
f
d
e
bc
c
WT
D1
D3
D7
(E)
TaIRO3
(+Fe)
(-Fe)
Relative Fold Change
14
12
10
8
6
4
2
0
a
b
a
c
a
d
a
e
WT
D1
D3
D7

Figure 8